This is a repository copy of *Adsorption of sterically-stabilized diblock copolymer nanoparticles at the oil–water interface: effect of charged end-groups on interfacial rheology*.

White Rose Research Online URL for this paper:
https://eprints.whiterose.ac.uk/196075/

Version: Supplemental Material

Article:
Chan, D.H.H., Hunter, S.J. orcid.org/0000-0002-9280-1969, Neal, T.J. orcid.org/0000-0003-4352-7024 et al. (3 more authors) (2022) Adsorption of sterically-stabilized diblock copolymer nanoparticles at the oil–water interface: effect of charged end-groups on interfacial rheology. Soft Matter, 18 (35). pp. 6757-6770. ISSN 1744-683X

https://doi.org/10.1039/d2sm00835a

Reuse
This article is distributed under the terms of the Creative Commons Attribution (CC BY) licence. This licence allows you to distribute, remix, tweak, and build upon the work, even commercially, as long as you credit the authors for the original work. More information and the full terms of the licence here: https://creativecommons.org/licenses/

Takedown
If you consider content in White Rose Research Online to be in breach of UK law, please notify us by emailing eprints@whiterose.ac.uk including the URL of the record and the reason for the withdrawal request.

eprints@whiterose.ac.uk
https://eprints.whiterose.ac.uk/

Electronic Supplementary Material (ESI) for Soft Matter.
This journal is © The Royal Society of Chemistry 2022

Supporting Information for:

Adsorption of Sterically-Stabilized Diblock Copolymer Nanoparticles at the Oil-Water Interface: Effect of Charged End-Groups on Interfacial Rheology

Derek H. H. Chan[a], Saul J. Hunter[a], Thomas J. Neal[a], Christopher Lindsay[b], Philip Taylor[b,*] and Steven P. Armes[a,*]

a. Dainton Building, Department of Chemistry, University of Sheffield,

Brook Hill, Sheffield, South Yorkshire, S3 7HF, UK.

b. Syngenta, Jealott's Hill International Research Centre, Bracknell, Berkshire, RG42 6EY, UK.

Summary of Contents

1. Further Experimental Details for the Synthesis of the (–) $PGMA_{54}$ and (+) $PGMA_{48}$ Precursors

Synthesis of Anionic (–) $PGMA_{54}$ Precursor by RAFT Solution Polymerization in Ethanol

GMA monomer (10.0 g, 62.4 mmol), PETTC RAFT agent (0.302 g, 0.892 mmol; target PGMA DP = 70), ACVA initiator (0.050 g, 0.18 mmol; PETTC/ACVA molar ratio = 5.0) and ethanol (15.5 g, 60% w/w) were weighed into a 100 mL round-bottom flask. The flask was cooled in an ice bath and degassed with N_2 gas for 30 min. Then it was immersed in an oil bath at 70 °C and the polymerization was quenched after 120 min by exposing the reaction mixture to air while cooling to 20 °C. ^{1}H NMR spectroscopy studies indicated a final GMA conversion of 77%. The reaction solution was diluted with methanol (10 mL) and then the crude polymer was precipitated into a ten-fold excess of dichloromethane (twice). The macro-CTA was dissolved in water and then freeze-dried overnight to afford a yellow powder. A mean DP of 54 was determined by end-group analysis via ^{1}H NMR spectroscopy (integrated aromatic proton signals at 7.2-7.5 ppm were compared to the methacrylic backbone protons at 0.7-2.5 ppm).

Synthesis of Cationic (+) $PGMA_{48}$ Precursor by RAFT Solution Polymerization in Ethanol

GMA monomer (10.0 g, 62.5 mmol), MPETTC RAFT agent (0.469 g, 1.04 mmol; target PGMA DP = 60), AIBA initiator (0.056 g, 0.21 mmol; MPETTC/AIBA molar ratio = 5.0) and ethanol (12.9 g, 55% w/w) were weighed into a 100 mL round-bottom flask. The flask was cooled in an ice bath and degassed with N_2 gas for 30 min. Then it was immersed in an oil bath set at 56 °C for 2 h before quenching the polymerization by exposing the reaction mixture to air while cooling the flask to 20 °C. ^{1}H NMR spectroscopy studies indicated a final GMA conversion of 80%. The crude polymer was purified by precipitation into a ten-fold excess of dichloromethane (twice). The purified precursor was dissolved in water and then freeze-dried to afford a yellow powder. A mean DP of 48 was determined by end-group analysis using ^{1}H NMR spectroscopy (integrated aromatic proton signals at 7.2-7.5 ppm were compared to the methacrylic backbone protons at 0.7-2.5 ppm).

2. Fourier transform of interfacial tension decay after a sudden expansion of a bubble

The interfacial dilatational response of an adsorbed layer can be determined using either an oscillatory deformation of the interface or via analysis of the interfacial tension decay (Δt) after a sudden expansion (ΔA). The sudden expansion of an equilibrated interface reduces the surface excess of the adsorbed material, leading to an increase in interfacial tension. This then decays over time back to its equilibrium value (see **Figure S1**).

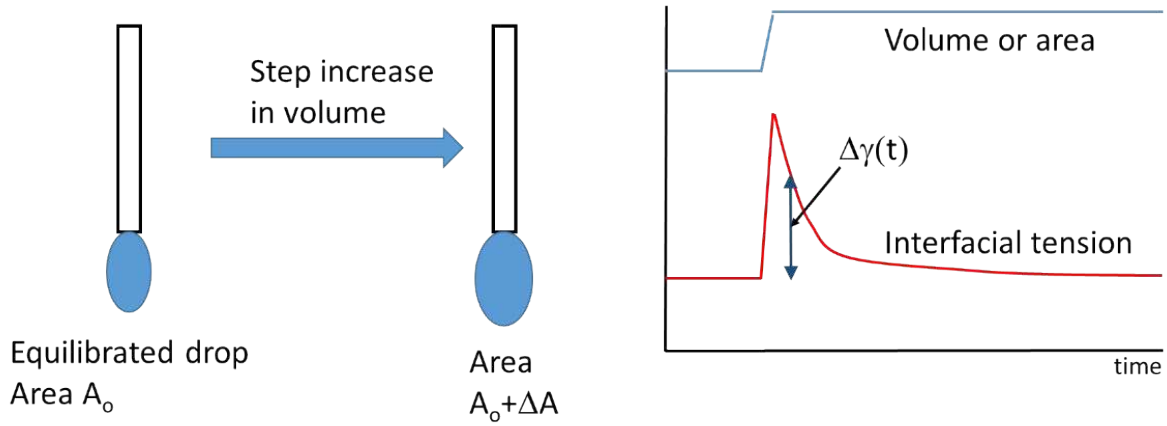

Figure S1. Schematic representation of a decay in interfacial tension after sudden expansion of an equilibrated interface (e.g. an aqueous droplet in the present study).

In principle, Fourier Transform (FT(x)) analysis of the time domain data obtained during the decay of the interfacial tension $\Delta\gamma(t)$ back to its equilibrium value can provide interfacial moduli in the frequency domain ($\varepsilon(\omega)$ where ω is the angular frequency). The Fourier transform for this process is given by:

$$\varepsilon(\omega) = \frac{FT(\Delta\gamma(t))}{FT(\Delta A(t))} = \frac{\int_0^\infty \Delta\gamma(t) e^{-i\omega t} dt}{\int_0^\infty \Delta A(t) e^{-i\omega t} dt} \qquad \text{S1}$$

The area change is a step function, $\Delta A(t)/A_o = 0$ $t \leq 0$ and $\Delta A(t)/A_o = \Delta A/A_o$ $t > 0$, hence

$$\int_0^\infty \frac{\Delta A(t)}{A_o} e^{-i\omega t} dt = \frac{\Delta A}{i\omega A_o} \qquad \text{S2}$$

The real component of $\varepsilon(\omega)$ relates to elastic properties ($\varepsilon'(\omega)$) and the imaginary component to loss properties ($\varepsilon''(\omega)$). Hence the integral shown in equation S2 can be split into these two components and the moduli evaluated from the decay function, $\beta(t)$, which is given by:

$$\beta(t) = A_o \Delta\gamma(t) / \Delta A \qquad \text{S3}$$

The decay of the interfacial tension, $\Delta\gamma(t)$, was recorded at increasing time intervals. This allowed sufficient resolution over short timescales after rapid expansion of the interface without requiring an excessively high frame rate over the whole decay measurement (20 000 s). The Fourier transform requires evenly spaced time points so the entire decay function was fitted to a triple exponential

decay to accurately reproduce the data using the non-linear triple exponential fitting routine in Origin v.6 (MicroCal). A further parameter, $\beta(\infty)$, was introduced when the interfacial tension had not fully relaxed back to its equilibrium value after 20 000 s. $\beta(\infty)$ is given by the following expression:

$$\beta(t) = \sum_{i=1}^{n} \beta(\infty) + A_i e^{-t/k_i} \qquad \text{S4}$$

Where n = 3. The Fourier transform equations shown above are reduced to give equations S5 and S6:

$$\varepsilon'(\omega) = \beta(\infty) + \omega \int_0^{\infty} (\beta(t) - \beta(\infty)) \sin(\omega t) dt \qquad \text{S5}$$

and

$$\varepsilon''(\omega) = \omega \int_0^{\infty} (\beta(t) - \beta(\infty)) \cos(\omega t) dt \qquad \text{S6}$$

Where $\varepsilon'(\omega)$ is the elastic (or storage) modulus and $\varepsilon''(\omega)$ is the viscous (or loss) modulus. For neutral (uncharged) nanoparticles, a high initial $\beta(0)$ value was observed so the decay function could not be satisfactorily fitted with a single triple exponential decay. In such cases, the decay curve was split into two time domains (typically 0-200 s and 200-20 000 s) and each domain was fitted separately. The decay function $\beta(t)$ was Fourier transformed by numerically integrating equations S5 and S6 over the frequency range 1 x 10^{-5} to 1 Hz (i.e., 6.28 x 10^{-5} to 6.28 rad s^{-1}) within Excel. A typical fitted data set using a single triple-exponential decay function obtained for a 0.1% w/w aqueous dispersion of (+) $PGMA_{48}$-$PMMA_{80}$ nanoparticles at pH 3 is shown in **Figure S2**.

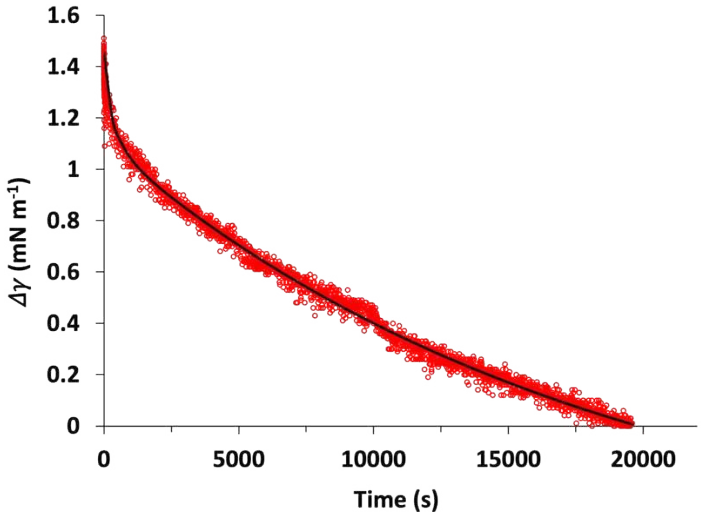

Figure S2. Example of a data fit to a single triple-exponential decay function obtained for a 20 mm^3 droplet immersed in *n*-dodecane, where the droplet phase comprises a 0.1% w/w aqueous dispersion of (+) $PGMA_{48}$-$PMMA_{80}$ nanoparticles at pH 3.

3. Oscillatory interfacial rheology

To confirm the interfacial relaxation experiments, oscillatory dilatation measurements were performed on 0.1% w/w aqueous dispersions of the (–) $PGMA_{54}$-$PMMA_{80}$ nanoparticles and (+) $PGMA_{48}$-$PMMA_{80}$ nanoparticles at pH 3 and pH 7 respectively, as well as for (0) $PGMA_{50}$-$PMMA_{80}$ nanoparticles at pH 7. In each case, these nanoparticles possess neutral character. Droplets (ca. 20 mm^3) of the aqueous nanoparticle dispersions were formed in *n*-dodecane (on a 1.65 mm outer diameter needle), equilibrated for 2 h and then subjected to oscillations corresponding to a relative area deformation of ca. 5% in the frequency range of ω = 0.0628 to 0.628 rad s^{-1} (i.e., 0.01 to 1 Hz) using a DataPhysics ODG20 tensiometer. The interfacial area, A(t), of such aqueous droplets was varied sinusoidally over time with an amplitude of ΔA about its mean value, A_o, such that

$$A(t) = A_o + \Delta A cos(\omega t) \quad \text{S7}$$

200 images were recorded for each droplet over time for five periods of oscillation at each frequency. Each image was analyzed using the instrument software to calculate the variation in interfacial tension with time, γ(t). The amplitude of the interfacial oscillation ($\Delta\gamma$) was determined and the variation in the interfacial tension during the oscillation is given by:

$$\gamma(t) = \gamma_o + \Delta\gamma cos(\omega t + \phi) \quad \text{S8}$$

Where ϕ is the phase angle between the sinusoidal variation in area and interfacial tension. The instrument software applies a Fourier transform to this variation to extract $\varepsilon'(\omega)$ and $\varepsilon''(\omega)$ at each frequency, where these parameters are given by the following expressions:

$$\varepsilon'(\omega) = \Delta\gamma(\omega)\frac{A_o}{\Delta A}cos\phi(\omega) \quad \text{S9}$$

And

$$\varepsilon''(\omega) = \Delta\gamma(\omega)\frac{A_o}{\Delta A}sin\phi(\omega) \quad \text{S10}$$

Typical plots of γ(t) and A(t) obtained for a 0.1% w/w aqueous dispersion of (0) $PGMA_{50}$-$PMMA_{80}$ nanoparticles are shown in **Figure S3**. There is only a small phase difference between the sinusoidal change in interfacial tension and the sinusoidal area curve, which suggests that the rheology is dominated by an elastic response at this frequency (0.628 rad s^{-1}).

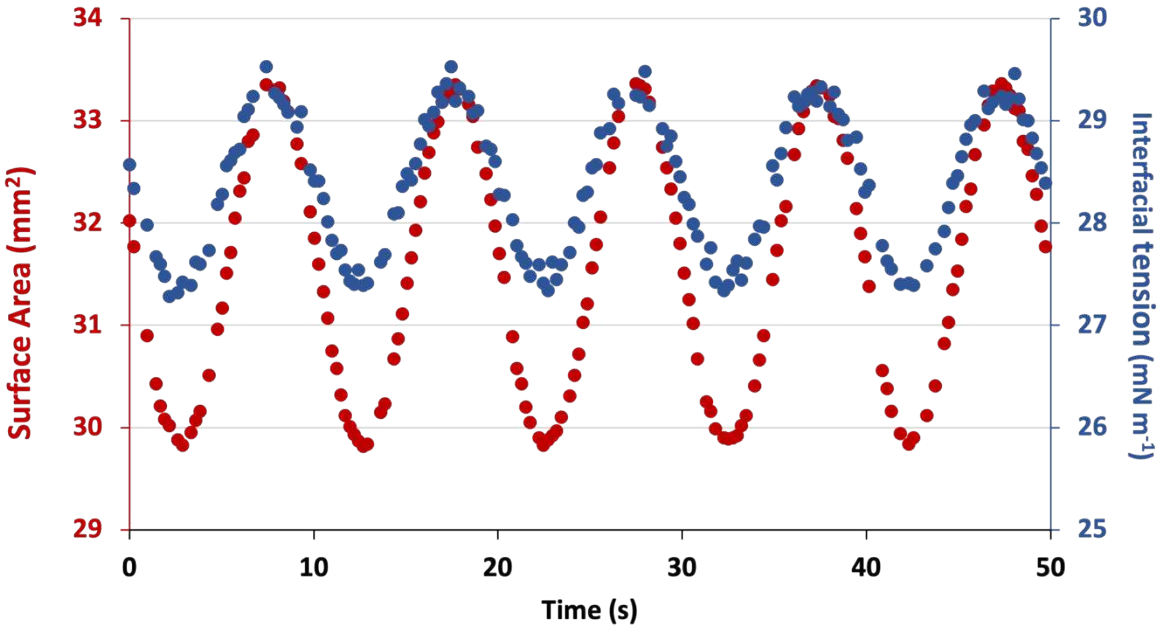

Figure S3. Variation in droplet surface area and interfacial tension observed over time at a frequency of 0.628 rad s^{-1} for (0) $PGMA_{50}$-$PMMA_{80}$ nanoparticles adsorbed at the *n*-dodecane/water interface.

Representative plots for $\varepsilon'(\omega)$ and $\varepsilon''(\omega)$ are shown in Figures S4 and S5 for dilute aqueous dispersions of the three types of nanoparticles at pH 3 and pH 7. Higher elastic moduli are always observed for neutral nanoparticles compared to cationic or anionic nanoparticles. These observations are consistent with the relaxation measurements and confirm that adjusting the solution pH has a significant effect on the interfacial adsorption of minimally-charged sterically-stabilized nanoparticles. Moreover, such moduli are only slightly lower than those calculated from the relaxation data, despite the significantly shorter equilibration times (2 h vs. overnight). This difference was readily apparent in the interfacial tension data, where the overnight equilibration values were generally 1-3 mN m^{-1} lower than those achieved after equilibration for 2 h. With the exception of the (+) $PGMA_{48}$-$PMMA_{80}$ nanoparticles at pH 7, all systems exhibited loss moduli of 0-2 mN m^{-1}, suggesting that no significant transfer of nanoparticles to or from the oil-water interface occurred over the timescale of the oscillations. Moreover, these very low values explain why loss moduli could not be determined from the relaxation measurements within this frequency region.

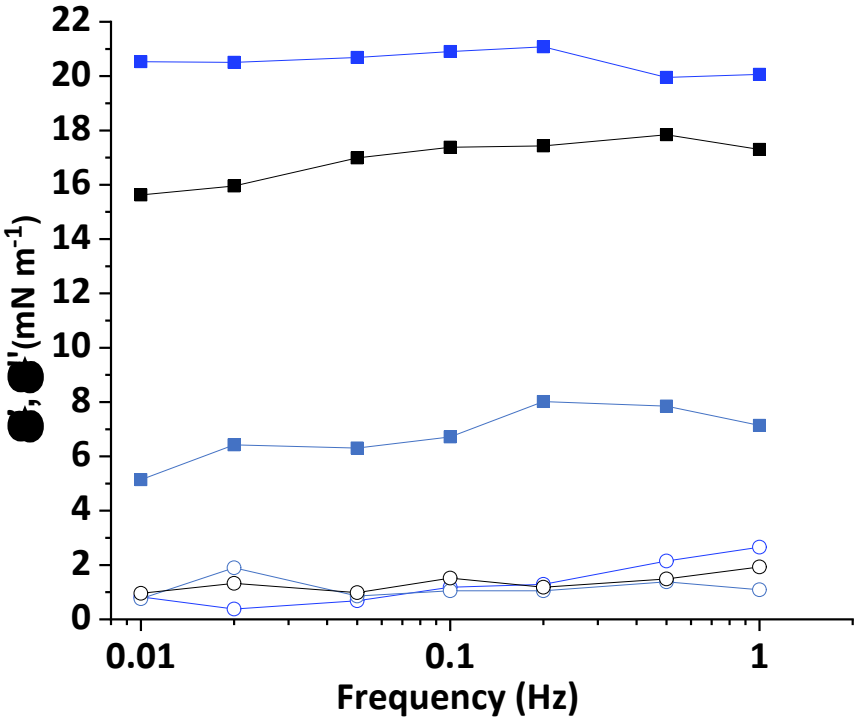

Figure S4. Frequency dependence for ε'(ω) and ε"(ω) observed for (0) $PGMA_{50}$-$PMMA_{80}$ nanoparticles (■ , o) and (–) $PGMA_{54}$-$PMMA_{80}$ nanoparticles (■ , o) at pH 7 and (–) $PGMA_{54}$-$PMMA_{80}$ nanoparticles (■ , o) at pH 3 adsorbed at the *n*-dodecane/water interface

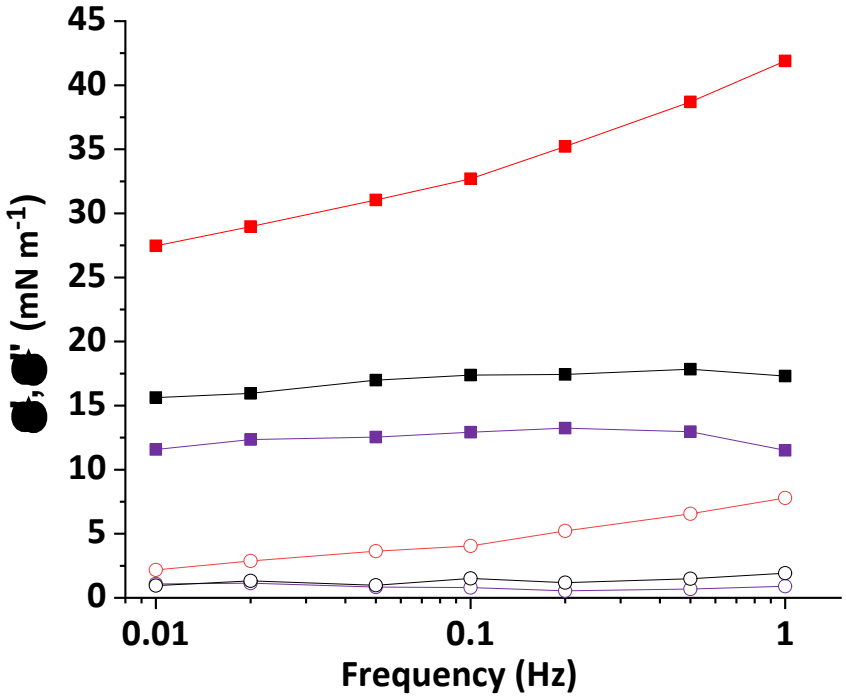

Figure S5. Frequency dependence for ε'(ω) and ε"(ω) observed for (0) $PGMA_{50}$-$PMMA_{80}$ nanoparticles (■ , o) and (+) $PGMA_{48}$-$PMMA_{80}$ nanoparticles (■ , o) at pH 7 and (+) $PGMA_{48}$-$PMMA_{80}$ nanoparticles (■ , o) at pH 3 adsorbed at the *n*-dodecane/water interface.

The interfacial properties determined for dialyzed and non-dialyzed (–) $PGMA_{54}$-$PMMA_{80}$ nanoparticles were compared at pH 7. Moduli for the dialyzed sample are 10-15% higher than those for the non-dialyzed sample. This difference was considered to be within experimental error hence non-dialyzed samples were used for the remaining experiments. A series of 10% w/w aqueous dispersions of nanoparticles were prepared and diluted to the desired concentration as required. Similar results were obtained for a freshly diluted sample of non-dialyzed (–) $PGMA_{54}$-$PMMA_{80}$ prepared at pH 7 compared to the same nanoparticles analyzed ten months previously. This suggests that such nanoparticles do not suffer hydrolytic degradation under such conditions.